Rheology of acid suspensions containing cassava bagasse: effect of biomass loading, acid content and temperature

Tiago Carregari Polachini [1,2]*; Antonio Mulet [2]; Juan A. Cárcel [2]; Javier Telis-Romero [1]

[1] Food Engineering and Technology Department, São Paulo State University (Unesp), Institute of Biosciences, Humanities and Exact Sciences (Ibilce), Campus São José do Rio Preto, São Paulo, 15054-000, Brazil.

[2] Grupo de Análisis y Simulación de Procesos Agroalimentarios (ASPA), Departamento de Tecnología de Alimentos, Universitat Politècnica de València (UPV), Valencia, 46071, Spain.

*Corresponding author: Fax: +55 (17) 3221-2250, Tel.: +55 (17) 3221-2251. E-mail: tiagopolachini@terra.com.br

Keywords: lignocellulose, residual starch, apparent viscosity, Herschel-Bulkley model, shear-thinning, Arrhenius-type equation.

1. Introduction

The widespread and non-sustainable use of fossil fuels is contributing to their exhaustion, besides damaging the environment by the emission of greenhouse gases. Developing and optimizing the second generation ethanol process has become increasingly interesting for producing biofuels from renewable sources. The adequate processing of biomass into bioethanol implies not only a reduction in CO_2 emissions throughout the fuel production chain but also an eco-friendly destination of the residues from agro-industrial processes. Such wastes are generally composed of macromolecules of cellulose, hemicellulose and lignin. Some of them can also present certain amounts of starch, protein, pectin and ash depending on the product, species, harvest conditions, processing and storage [1]. The variability in its composition reinforces the importance of specifically evaluating the performance of each potential biomass for a given process.

Cassava (*Manihot esculenta*) is one of the main raw materials used in the starch extraction industry, where cassava bagasse appears as a valuable and abundant byproduct. Currently, in Brazil alone, approximately 2 million tons of wet bagasse per year are generated, [2, 3]. The differential for cassava bagasse in relation to other residues is associated with its high residual starch content which is a consequence of the low yield of cassava starch extraction [4], which can range from approximately 30 up to 85% (in dry basis) according to the literature [5, 6].

Due to its specific chemical composition, cassava bagasse is a potential raw material for bioethanol production. However, well designed pretreatment and hydrolysis needs to be carried out to access the entangled starch and the complex structure of cellulose and hemicellulose. The conversion efficiency of these main macromolecules into small chain carbohydrates must be characterized by high sugar production with low formation of sugar degradation compounds. This can be attained by pretreating the biomass under mild temperatures, using less aggressive acids and under easy-mixing conditions. Phosphoric acid, for example, is able to hydrolyze both lignocellulosic and starchy biomass with reduced sugar degradation [7, 8]. Its use at low temperatures can also prevent the starchy suspension from gelatinizing, which would decrease the mass transfer and the yield of cold hydrolysis of starch granules.

In addition to the technological issues, the process efficiency is highly dependent on the correct design of equipment and unit operations. The properties of the raw material is the fundamental information needed to optimize the industrial process. Properties, such as the rheological ones, allow an adequate choice of pumps, accessories, mixers, bioreactors and pipes [9]. However, the study of the properties demands more efforts for the case of heterogeneous aqueous systems which may be influenced by the different amounts of insoluble (biomass particles) and soluble (acid) compounds. While particles can have different sizes and aspect ratios, the presence of an acid can affect how the particles interact with each other during the flow [10, 11].

Consequently, the way each of the factors listed above influences the rheological behavior of dilute acid suspensions of cassava bagasse needs to be investigated. Steady-flow curves provide useful data not only for the rheological modelling but also for evaluating the transition between Newtonian and non-Newtonian behavior. Modifications in the suspension compositions may turn Newtonian fluids into viscoplastic fluids with significant initial stress to start the flow, pseudoplastic (or shear-thinning) or dilatant (or shear-thickening) fluids in the presence or absence of yield stress. On the one hand, the shear-thinning fluids show decreasing apparent viscosity as the shear rate is increased. On the other hand, the apparent viscosity of the shear-thickening ones tends to increase with increasing shear rate. Distinct systems may need different sources of energy to attain similar pretreatment conditions, even more so when they include non-conventional techniques such as high-intensity ultrasound. For example, suspensions concentrated in biomass tend to require more energy input to reach the same acoustic effect ~~power obtained~~ in dilute suspensions [12], which is probably related to the increased viscosity [9].

Therefore, this study focused on determining and modelling the rheological behavior of different acid suspensions containing previously-characterized cassava bagasse.

2. Materials and Methods

2.1. Cassava bagasse and suspension preparation

Coarsely particulate, dried cassava bagasse was kindly provided by TechnoAmido (São Pedro do Turvo, Brazil). These coarse particles were ground using an M4FH1C knife mill (PHD, Piracicaba, Brazil) at 1750 rpm and then the powdered bagasse was standardized using a sieve (Tyler mesh 100) in order to obtain particles smaller than 0.147 mm.

Dilute acid suspensions were prepared varying the phosphoric acid (85% solution; purity>99.95%), (Dinâmica, Diadema, São Paulo), content in distilled water at the following concentrations: 0, 2, 4, 6, 8 and 10% (g of acid per 100 g of dispersant). These solutions were added to cassava bagasse to obtain suspensions with final solids concentrations of 0, 2, 4, 6, 8 and 10% (g of cassava bagasse per 100 g of suspension). Combining the 6 acid solutions with the 6 cassava bagasse concentrations resulted in a total of 36 samples to be analyzed.

2.2. Cassava bagasse characterization

2.2.1. Chemical composition

The cassava bagasse was characterized according to its chemical composition, in triplicate, by determining the protein content by the micro-Kjeldahl method, fat content by Soxhlet extraction, ash content by muffle incineration and moisture content in an oven according to AOAC [13]. Among the carbohydrates, starch content was quantified in a similar way to that described by Paul et al. [14], total fiber content was quantified by the method proposed by Van Soest et al. [15] and total soluble sugars was found by difference. Moreover, the fractions of cellulose, hemicellulose and lignin in the lignocellulose were determined based on the values of insoluble fibers in acid (ADF) and neutral detergent (NDF).

2.2.2. Particle size

Particle size of the powdered cassava bagasse was determined in triplicate by laser diffraction (LD) using a MAM 5005 Mastersizer (Malvern Panalytical, Malvern, UK). Distilled water was used as the dispersing medium for the measurements. In this technique, the particles scatter light at an angle of diffraction which is considered inversely proportional to their size. The particle size distribution is initially measured based on volume, expressing the volume percentage of particles in continuous size intervals. Making use of these values, the number-based distribution can be determined by the equivalent sphere assumption.

The diameter of the samples was represented as the volume weighted mean diameter ($D_{4,3}$), also known as the De Brouckere mean diameter, defined by Equation (1), and surface weighted mean diameter ($D_{3,2}$) or the so-called Sauter mean diameter, defined by Equation (2). The De Brouckere mean diameter assumes spherical particles of the same volume as the actual particles, while the Sauter mean diameter is defined as the diameter of the sphere with the same surface area as the particle [16]. Polydispersity (width of distribution) was also evaluated according to span value, given in Equation (3). All of them were calculated with respect to the volume-based and number-based distributions.

$$D_{4,3} = \frac{\sum n_i \cdot d_i^4}{\sum n_i \cdot d_i^3} \quad (1)$$

$$D_{3,2} = \frac{\sum n_i \cdot d_i^3}{\sum n_i \cdot d_i^2} \quad (2)$$

$$\text{span} = \frac{D_{0,9} - D_{0,1}}{D_{0,5}} \quad (3)$$

where, n_i is the number of particles with d_i diameter (μm), $D_{0,1}$, $D_{0,5}$ and $D_{0,9}$ are additional parameters given by the instrument which represent the maximum particle diameter below which 10%, 50% and 90% of the sample exists, respectively.

2.2.3. Particles morphology

The morphology of cassava bagasse particles was evaluated using a BX43 optical microscope (Olympus, Tokyo, Japan) with coupled camera at 4x, 10x and 40x magnitude. Samples were dispersed in distilled water for glass slide preparation and images were acquired from different areas on the microscope slides. In order to identify and to show the presence of residual starch, the bagasse was marked with lugol solution.

Besides the visual analyses, particles were also characterized according to the aspect ratio (a_r) given by the relation between length (L) and width (w). Measurements of such characteristic dimensions were done for 100 particles in the different fields of view using the cellSens software version 1.18 (Olympus, Tokyo, Japan).

2.3. Rheological measurements

Rheological measurements were carried out in triplicate using an AR-G2 rotational rheometer (TA Instruments, New Castle, USA) with the SPC (Starch Pasting Cell) geometry. This vane-type geometry was used in order to avoid particle sedimentation and slip effects [17]. Approximately 28 mL of each sample were inserted into the equipment and shear rate ramps were set from 1 to 265 s^{-1} in steady flow with 10 points per logarithm interval. The rheological experiments were conducted at five different temperatures: 278.13, 288.13, 298.13, 308.13 and 318.13 K, using a controlled temperature bath and a new sample for each assay. Data of shear stress were obtained from Universal Analysis 2000 data acquisition system version 4.7 (TA Instruments, New Castle, USA).

2.4. Modelling

The means of the triplicate experimental values of the shear stress obtained at each fixed shear rate were calculated for the 36 samples at the temperatures of 278.13, 288.13, 298.13, 308.13 and 318.13 K. Average data of shear stress were plotted against shear rate to obtain the corresponding rheograms. The Newton (Equation 4), Bingham (Equation 5), Power Law (Equation 6) and Herschel-Bulkley (Equation 7) models were used to analyze the rheological behavior:

$$\tau = \mu\dot{\gamma} \quad (4)$$

$$\tau = \tau_0 + \eta_B\dot{\gamma} \quad (5)$$

$$\tau = k\dot{\gamma}^n \quad (6)$$

$$\tau = \tau_0 + k\dot{\gamma}^n \quad (7)$$

In these equations, τ (Pa) is shear stress, $\dot{\gamma}$ (s^{-1}) is shear rate, μ (Pa·s) is the Newtonian viscosity, τ_0 (Pa) is the yield stress, η_B (Pa·s) is the plastic viscosity, k (Pa·s^n) is the consistency coefficient and n (dimensionless) is the flow behavior index. Fluids with flow behavior index below 1 correspond to shear-thinning fluids while values above 1 indicate shear-thickening behavior. The rheograms were fitted to the Herschel-Bulkley model in order to estimate and to evaluate the rheological parameters, the presence of yield stress and shear-thinning or shear-thickening behavior. The apparent viscosity η_{app} (Pa·s) at a fixed shear rate can be determined from the values of μ after equalizing the shear stress of a non-Newtonian model to the Newton model [18]. The OriginPro 8.0 software (OriginLab Corporation, Northampton, USA) was used to plot the graphs and to carry out the non-linear regressions.

The parameters from the Herschel-Bulkley model were submitted to estimated effects analysis and to the analysis of variance using the STATISTICA 10 software (StatSoft Inc., Tulsa, USA) in order to study the influence of the variables on the rheological parameters. The significance of the linear and quadratic terms of cassava bagasse concentration (X_S, %), phosphoric acid content (X_A, %) and absolute temperature (T, K) were analyzed as well as the possible linear interaction among them. The significant variables ($p < 0.05$) were used to fit the data and provide a final version of the predictive equation for each parameter. The accuracy of fit was evaluated through the adjusted determination coefficient (R_{adj}^2), which is a modification of the conventional determination coefficient R^2 to take into account the number of parameters of the fitted model, and by the root mean square error (*RMSE*), given respectively by Equation (8) and Equation (9):

$$R_{adj}^2 = 1 - \frac{(m-1)}{(m-p-1)}\left(1 - R^2\right) \tag{8}$$

$$RMSE = \sqrt{\frac{\sum_{m=1}^{m}\left(\hat{y}_m - y_m\right)^2}{m}} \tag{9}$$

where m is the number of experimental data, p the number of parameters in the model, R^2 is the determination coefficient, $\hat{y}_m$ the predicted data and y_m the experimental data.

The effect of temperature on the apparent viscosity of the suspensions was modelled by an Arrhenius-type equation (Equation 10):

$$\eta_{app,10s^{-1}} = A_0 \exp\left(\frac{E_a}{RT}\right) \tag{10}$$

where A_0 is the pre-exponential factor (Pa·s), E_a is the activation energy (J·mol^{-1}) and R is the universal gas constant (8.314 J·mol^{-1}·K^{-1}).

3. Results and discussion

3.1. Chemical characterization

Cassava bagasse samples were chemically characterized (Table 1). The samples have considerable amounts of residual starch around 50% (in dry basis). This agrees with results reported by other authors of residual starch in cassava bagasse ranging from 30%

up to 85% (in dry basis) [4, 5]. Starch is a polymer with great capacity for releasing fermentable matter. After being hydrolyzed, it can be used as substrate for many applications, including for second generation ethanol production.

Similarly as reported by Polachini et al. [19] and Silva et al. [20], the cassava bagasse also showed low fat, ash and protein content. As a consequence of the low concentration of high-value nutrients, cassava bagasse is not often used for animal feed. Consequently, the higher carbohydrate content makes it advantageous for microbial conversion when compared to other residues [4].

Fibers represented 46.1% of the bagasse, approximately 92% being cellulose and hemicellulose. In addition to the capacity for releasing sugar from starch, low molecular weight carbohydrates can also be obtained in large amounts from the fibrous matter. Lu et al. [21] showed the high production of glucose and lower amounts of xylose and arabinose from the hydrolysis of starch and lignocellulose from cassava bagasse. On the other hand, it is known that the presence of lignin makes the hydrolyzation of cellulose and hemicellulose difficult. Thus, the low content of lignin observed in cassava bagasse fibers (≈ 8%) offers advantages in contrast with other residues such as sugarcane bagasse, rice straw, corn stover and wheat straw, which all showed 14–23% lignin by dry weight [22].

3.2. Particles size determination

Figure 1 shows the particle size distribution, where a monomodal distribution can be seen for both volume-based and number-based distribution.

Table 2 presents the average values of the different diameters as well as the span values obtained from the volume-based and number-based distributions. According to the $D_{0,9}$ from the number-based distribution, powdered cassava bagasse presented the majority

(90%) of particles with particle size smaller than 6.1 µm. However, probably, the presence of a few bigger particles (fibers and agglomerates) resulted in a volume weighted mean diameter ($D_{4,3}$) of approximately 120 µm

Concerning the volume-based distribution, the average volume-weighted mean diameter ($D_{4,3}$) was 175 µm. On the other hand, the values for surface-weighted mean diameter $D_{3,2}$ (~60 µm) were much lower than $D_{4,3}$ probably due to the presence of longer, thinner particles instead of more rounded ones [9]. According to Glaser [23], $D_{3,2}$ is an efficient parameter for evaluating hydrolysis performance of non-homogeneous substrates. The same author also stated that biomass with particle size below 200 µm is more accessible to cellulases for further conversion. Consequently, cassava bagasse is an adequate substrate for cellulases since all the mean diameters obtained were lower than this value. A slightly higher span value of 1.935 was a consequence of the varied particle sizes, which can be seen in Figure 1. Moreover, 10% of the volume occupied by the particles ($D_{0,1}$) is attributed to particles smaller than 40 µm and 90% of the volume occupied ($D_{0,9}$) corresponds to particles smaller than 340 µm. Thus, it can be assumed that that 80% of the occupied volume is linked to particles with mean diameter between 40 µm and 340 µm. This observation reinforced the difference between the two distributions, which means that more small particles are necessary to occupy the same volume as bigger ones.

3.3. Morphological characteristics

Figure 2 shows particles with varied morphologies such as round, rectangular and elongated shapes in the micrographs at different magnifications. They are typical of cellulosic residues, with irregular form and the possible presence of microfibers. Similar structures have been reported in the literature for peanut shells [9], sugarcane bagasse [24] and even cassava bagasse [25]. In addition to the cellulosic particles, there were also starch granules (black arrows in Figure 2a). Figure 2b shows the cassava bagasse marked with lugol, where the bluish-purple structure indicated starch with iodine. It could be seen that some starch was in the form of granules dispersed or entangled in the fibrous network, which was also observed by Versino et al. [26] and Odoch et al. [27] using scanning electronic microscopy of cassava bagasse. Another fraction seemed to be solubilized as amylose and amylopectin, probably as a result of a partial starch gelatinization and leaching during the cassava processing. The bluish areas also reflect the difficulty in recovering all the cassava starch during its extraction process.

The aspect ratio (a_r) of the samples was also determined from the microscopic images. Mean aspect ratio of the sample was found to be 1.98, being the distribution of the aspect ratio shown in the histogram in Figure 3. More than 60% of the particles analyzed had aspect ratios in the range between 1 and 2.5 , which is similar to the mean values and the data reported for other agro-industrial residues [28]. The presence of starch granules in relatively spherical form leads to a high concentration of particles with an aspect ratio near to 1.

3.4. Flow behavior

The mean shear stress was calculated in all samples for each fixed shear rate at the different temperatures. An average value of the relative standard deviations (standard deviation/mean shear stress) were also calculated in a given flow condition, being these values lower than 3.86% in all of the measurements regarding the 36 samples at the different temperatures. The values obtained were in the range from 0.001 Pa to 8.181 Pa at 1.01 s^{-1} and from 0.184 Pa to 604.91 Pa at 263.34 s^{-1}. In general, as shown in Figure 4, shear stresses increased with the increase of cassava bagasse and acid content and the lowering of temperature. An off-trend displacement was observed between the flow curves of 8% and 10% of solids in Figure 4a, 8% and 10% of acid concentration in Figure 4b and of 308.13 K and 318.13 K n Figure 4c. It indicates that some non-linear trend occurred when solids loading, acid concentration and temperature were varied.

Figure 4 also shows some rheograms fitted to the Herschel-Bulkley model for different solids concentration, acid content and temperature. In Table 3, some fitting parameters for acid suspensions at intermediate concentration of solids, acid content and temperatures are shown. Full data are provided as Supplementary File (Table S1)

Although all data were well-fitted to Herschel-Bulkley model (R^2>0.998), not all fitting parameters presented large values or physical meaning. For example, acid solutions and suspensions with solids content up to 4% showed relatively low yield stresses (τ_0) and flow behavior index (n) very close to 1. In these conditions, the Herschel-Bulkley model turns into the Newton model and the consistency coefficient can be considered as Newtonian viscosity. Coussot [29] assumed that the interactions between biomass particles are negligible in suspensions with low concentration of solids (< 4%), with Newtonian-like behavior of the dispersant medium predominating.

When the solids content and the phosphoric content was 6%, non-Newtonian behavior was more marked. It occurred for suspensions containing powdered peanut shells at higher solids concentration (8%) [9]. Besides the phosphoric acid, the main differences that could be linked to the different types of biomass can be attributed to the chemical composition and to the mean particle size ($D_{3,2}$ = 178.46 µm for peanut shells and $D_{3,2}$ = 66.3 µm for cassava bagasse), since the aspect ratio was quite similar. Peanut shells are mainly lignocellulosic material while the cassava bagasse is composed by considerable amounts of starch granules and this difference may affect compressibility and frictional forces between the matrices structure [30]. Hou et al. [31] also reported higher apparent viscosities for suspensions containing smaller particles in comparison with suspensions constituted by bigger particles, probably due to an increased specific surface area of thinner particles and the consequent higher particles interaction [32].

Regarding the rheological parameters, it was noticed that the yield stress (τ_0) increased and the values of the flow behavior index (n) decreased when phosphoric acid or cassava bagasse concentrations were higher. At the lower temperature with the highest acid and solids concentration the highest τ_0 value (3.21) and the lowest n (0.85) were found. These values are in accordance with previous studies for both lignocellulosic and starchy materials, which fitted the Herschel-Bulkley model to suspensions containing corn stover, peanut shells and amaranth starch [9, 33, 34] with similar trends. As reported in the literature, suspensions containing biomass generally present shear-thinning behavior with significant yield stress when approximately 5% of solids is attained [11]. This trend is likely due to the increased interparticle friction when decreasing the content of interstitial solvent, which influences not only the required energy for starting the flow but also how significant is the particles and aggregates reorganization when shear rate is changed.

The maximum value observed for yield stress was approximately 3.22 Pa, indicating that the most concentrated suspensions tested in this work were still able to be mixed by traditional stirred tanks instead of specialized reactors. Roche et al. [35] stated that suspensions with yield stress up to 10 Pa behave as pourable liquids, instead of paste-like characteristics with complex transport properties. These conditions promote the acid-particle interactions since the catalyst is more adequately and uniformly distributed in the dispersant when compared to concentrated materials [33]. In this context, the energy required for moving the materials increases with increasing solids content. The consistency coefficient can increase up to approximately 20 times (from 0.25 to 4.96 $Pa \cdot s^n$) when the solids concentration varies from 2% to 10% (5 times).

In addition to the visible effect of the variables on rheological parameters, an analysis of the estimated effects was carried out to evaluate its significance ($p < 0.05$ confirmed by the analysis of variance in Tables S2, S3, S4 and S5 from the Supplementary File). In general, yield stress (τ_0) and consistency coefficient (k) were linearly affected by all variables. Additionally, significant quadratic effects were observed for temperature and biomass concentration, besides the linear interaction $X_S T$ and $X_S X_A$, on both τ_0 and k. On the other hand, flow behavior index (n) was linearly affected by the biomass and acid contents and by the linear interaction between them. Solids content also had a quadratic effect on n, with no significant influence of temperature.

Apparent viscosity ($\eta_{app,10s^{-1}}$) was calculated at specific shear rate of 10 s^{-1}, which is considered adequate for a mixing and stirring process [18, 33]. It ranged from 7.07×10^{-4} Pa·s for the pure water at 318.13 K up to 3.82 Pa·s for the most solid and acid concentrated suspension at 278.13 K. These values were linearly influenced by all variables with an additional quadratic effect of temperature. The linear interactions $X_S T$ and $X_S X_A$ were also significant, similar to τ_0 and k.

In this way, non-linear regression can be done for each rheological parameter as a simultaneous function of the significant variables. Equation (11), Equation (12), Equation (13) and Equation (14) that follow were well-fitted to yield stress, consistency coefficient, flow behavior index and apparent viscosity. They had the fitted determination coefficient (R^2_{adj}) equal to 0.8596, 0.9744, 0.9392 and 0.9677, and the root mean square error equal to 0.28 Pa, 0.19 Pa·s^n, 0.01 and 0.17 Pa·s, respectively:

$$\begin{aligned}\tau_0 = 25.48 - 0.177T + 0.00031T^2 + 1.2648X_S - 0.00471X_S^2 \\ + 0.06515X_A - 0.00371X_S T + 0.00834X_S X_A\end{aligned} \quad (11)$$

$$\begin{aligned}k = 25.49 - 0.179T + 0.00031T^2 + 1.8991X_S - 0.01222X_S^2 \\ + 0.05198X_A - 0.00591X_S T + 0.00756X_S X_A\end{aligned} \quad (12)$$

$$n = 0.9987 + 0.006588X_S - 0.001617X_S^2 + 0.000187X_A - 0.000553X_S X_A \quad (13)$$

$$\eta_{app,10s^{-1}} = 24.09 - 0.16795T + 0.00029T^2 + 1.70511X_S + 0.066X_A - 0.00497X_S T + 0.00296X_S X_A \quad (14)$$

In any acid solutions and acid suspensions with solids concentration lower than 6%, yield stress values can be disregarded ($\tau_0 \approx 0$), the flow behavior index can be approximated to unity ($n \approx 1$) and both k and $\eta_{app,10s^{-1}}$ can be considered as for the Newtonian viscosity.

3.4.1. Solids concentration

Figure 5 shows the yield stress, consistency coefficient and flow behavior index as functions of cassava bagasse concentration. These graphs are in accordance with the previous analyses of variance, presenting the linear and quadratic effect of biomass on all rheological parameters.

The values of yield stress increased as the solids concentration increased. Although authors correlate yield stress with solids concentration by a power relation [11], Laera et al. [36] states that a linear tendency can be assumed in the case of diluted suspensions. The yield stress information is useful since it corresponds to the initial energy needed to move biomass suspensions. The way yield stress behaves as solids concentration changes can provide important information about the increase in power requirements when particle settling occurs before the mixer starts moving [11].

A similar trend was also observed for the consistency coefficient and for apparent viscosity. Higher values were obtained with increasing biomass content probably due to more particle-particle interaction during the flow as a consequence of the number of particles and the reduction of dispersant as it is absorbed causing the particles to swell [22]. In addition, mechanical energy is also dissipated by the dispersant when it flows around the particles when they appear in slightly higher concentrations [37].

The flow behavior index had a non-linear decrease as the solids concentration increased. The drop in the *n* values reflects the decrease in apparent viscosity as the shear rate increased. Polachini et al. [9] related the shear-thinning behavior to the increasing number of collisions among the particles in high loaded suspensions and a consequent deviation from Newtonian properties. Moreover, the breakdown of the aggregate as the shear rate increases can promote the release of interstitial dispersant and particles alignment, providing easy-flow characteristics and the reduction in apparent viscosity values.

3.4.2. Phosphoric acid content

The acidification of the medium also had significant influence on the rheological parameters. Figure 6 shows the effect of H_3PO_4 concentration on rheological behavior for different acid suspensions. While the yield stress, consistency coefficient and apparent viscosity increased linearly with increasing acid concentration, the flow behavior index seemed to present a slight less pronounced linear decrease as acid content was increased. The apparent viscosity of the acid solutions increased linearly with increasing acid content. Furthermore, Pääkkö et al. [10] stated that the negative charges of hemicellulose can be neutralized by the H+ ions. This might reduce electrostatic repulsion among the particles, which leads to an increase in the interfibrillar action and, consequently, in the suspension viscosity. Also, this increase in the particle-particle interaction seemed to slighty enhance the shear-thinning behavior in the higher loaded samples. This could be due to higher particle aggregation and the consequent release of the water trapped within the aggregates at higher shear rates.

3.4.3. Temperature dependence

Temperature had significant influence on yield stress, consistency coefficient and apparent viscosity but no effect on the flow behavior index. The values of τ_0, k and $\eta_{app,10s^{-1}}$ tended to decrease significantly as the temperature increased (Figure 7). The resistance to flow decreased as a consequence of the increase in the degree of molecular thermodynamic movement with increasing temperature. Increasing the temperature keeps the particles away from each other which reduces both viscosity and the specific mass of liquid materials. A similar trend was observed for microalgae slurries and peanut shell suspensions over similar temperature ranges [9, 37].

Although the analyses of variance showed quadratic influence of temperature on τ_0, k and $\eta_{app,10s^{-1}}$, the literature usually correlates the effect of temperature on rheological parameters by an Arrhenius-type equation. Thus, the activation energy of the Arrhenius equation reflects the temperature dependence of each sample. In other words, suspensions with higher E_a have more pronounced variation in viscosity for the same temperature change when compared to the ones with lower E_a.

The fitting parameters of an Arrhenius-type equation are shown in Table 4. The goodness of fit was measured by R^2_{adj}, achieving values greater than 0.8603 for all samples. Ségalen et al. [38] demonstrated that slurries such as sludge follow an Arrhenius-type behavior when they are fully broken, i. e., when non-hydrodynamic forces can be neglected by applying enough shear rate. It means that the suspensions at the studied conditions in our work presented liquid-like characteristics, its transport being easier when compared to solid-like fluids.

The flow activation energy of the acid solutions ($X_S = 0\%$) resulted in higher values than the ones for acid suspensions, even presenting a slight decrease with increasing acid concentration. These values are in close agreement with the range established for pure water (13 up to 16 $kJ \cdot mol^{-1}$) [39], as it was the major component. These values indicated that the dispersants had their apparent viscosity more strongly affected by temperature in relation to the suspensions. Krokida et al. [40] stated that the addition of non-soluble solids, such as fibers, in the suspensions implies lower E_a when compared to water.

The addition of biomass particles to an acidified medium can increase the number of hydrogen bonds related to, e. g. the carboxyl groups in the hemicellulose and hydroxyl groups in the amylose and amylopectin. The higher sensitivity of apparent viscosity with increasing solids content can be linked to the structural changes of the aggregates as a consequence of the buildup or breakdown of the hydrogen bonding and hydrophobic interactions when temperature is altered [41]. Analogously, it could be seen that E_a of the suspensions tend to decrease as the acid concentration increased, probably due to the neutralization of the carboxyl and hydroxyl groups by the H^+ ions.

In the aqueous suspensions ($X_A = 0\%$), the activation energy tended to decrease when the solids content increased. The absence of hydrogen ions may raise difficulties in establishing hydrogen bonds among the molecules, leading to charge repulsion by the particles. In addition, the high number of small particles in powdered cassava bagasse could act like a dispersant to facilitate the flow of coarser particles. This phenomenon, observed by Farris [42], could explain the reduced required flow energy as the suspensions become more concentrated.

4. Conclusions

The high content of residual starch (~49%) and cellulose and hemicellulose (total of ~43%) in the dried bagasse highlighted the need for an adequately designed conversion process not only for converting entangled and dispersed residual starch but also the fermentable matter of lignocellulose. In order to provide important information for the design of equipment and plant operations, rheological behavior of different acid suspensions was studied as a function of solids concentration (0–10%), phosphoric acid in the solution (0–10%) and temperature (278.13–318.13 K). Samples with less than 6% of solids presented Newtonian behavior while the more concentrated ones (≥6%) behaved as non-Newtonian fluids with noticeable yield stress (0 Pa < τ_0 < 3.22 Pa) and shear-thinning characteristics (0.85 < n < 1).

Resistance to the flow (τ_0, k and $\eta_{app,10s^{-1}}$) was increased by increasing cassava bagasse loading, acid content and decreasing temperature. Flow behavior index (n) decreased as the biomass and acid concentration increased but no effect of temperature was noticeable. For the range of variables considered, polynomial models could be fitted to provide ready-to-use information. Under the studied conditions, suspensions showed liquid-like properties. These facilitate the mass transport and the access of enzymes when compared to high concentrated pastes. Additionally, in these conditions, hydrolysis and further additional treatments can be enhanced since these conditions allow more efficient propagation of ultrasound in conversion processes assisted by non-conventional technologies.

5. Acknowledgment

The authors would like to thank Prof. Rosiane Lopes Cunha and Prof. Ana Carla Kawazoe Sato from University of Campinas (UNICAMP) for their support with particle size analyses. The authors also acknowledge the São Paulo Research Foundation – FAPESP (Grant number 2017/06518-2) and the Coordination for the Improvement of Higher Education Personnel – CAPES (Grant number 88881.132626/2016-01) for their financial support.

6. References

[1] K.L. Kenney, W.A. Smith, G.L. Gresham, T.L. Westover, Understanding biomass feedstock variability, Biofuels, 4 (2013) 111-127.

[2] F.A. Fiorda, M.S.S. Soares-Jr, F.A. Silva, L.R.F. Souto, M.V.E. Grossmann, Farinha de bagaço de mandioca: aproveitamento de subproduto e comparação com fécula de mandioca, Pesquisa Agropecuária Tropical, 43 (2013) 408-416.

[3] FAO, Official data of cassava production, Food and Agriculture Organization of the United Nations, 2019.

[4] A. Pandey, C.R. Soccol, P. Nigam, V.T. Soccol, L.P.S. Vandenberghe, R. Mohan, Biotechnological potential of agro-industrial residues. II: cassava bagasse, Bioresource Technology, 74 (2000) 81-87.

[5] D. Pasquini, E.M. Teixeira, A.A.S. Curvelo, M.N. Belgacem, A. Dufresne, Extraction of cellulose whiskers from cassava bagasse and their applications as reinforcing agent in natural rubber, Industrial Crops and Products, 32 (2010) 486-490.

[6] A.S. Sánchez, Y.L. Silva, R.A. Kalid, E. Cohim, E.A. Torres, Waste bio-refineries for the cassava starch industry: New trends and review of alternatives, Renewable and Sustainable Energy Reviews, 73 (2017) 1265-1275.

[7] S. Gámez, J.J. González-Cabriales, J.A. Ramírez, G. Garrote, M. Vázquez, Study of the hydrolysis of sugar cane bagasse using phosphoric acid, Journal of Food Engineering, 74 (2006) 78-88.

[8] P. Lenihan, A. Orozco, E. O'Neill, M.N.M. Ahmad, D.W. Rooney, G.M. Walker, Dilute acid hydrolysis of lignocellulosic biomass, Chemical Engineering Journal, 156 (2010) 395-403.

[9] T.C. Polachini, A.C.K. Sato, R.L. Cunha, J. Telis-Romero, Density and rheology of acid suspensions of peanut waste in different conditions: An engineering basis for bioethanol production, Powder Technology, 294 (2016) 168-176.

[10] M. Pääkkö, M. Ankerfors, H. Kosonen, A. Nykänen, S. Ahola, M. Österberg, J. Ruokolainen, J. Laine, P.T. Larsson, O. Ikkala, T. Lindström, Enzymatic Hydrolysis Combined with Mechanical Shearing and High-Pressure Homogenization for Nanoscale Cellulose Fibrils and Strong Gels, Biomacromolecules, 8 (2007) 1934-1941.

[11] J.J. Stickel, J.S. Knutsen, M.W. Liberatore, W. Luu, D.W. Bousfield, D.J. Klingenberg, C.T. Scott, T.W. Root, M.R. Ehrhardt, T.O. Monz, Rheology measurements of a biomass slurry: an inter-laboratory study, Rheol Acta, 48 (2009) 1005-1015.

[12] T.C. Polachini, G.R.d. Carvalho, J. Telis-Romero, Determination of acoustic fields in acidic suspensions of peanut shell during pretreatment with high-intensity ultrasound, Brazilian Journal of Chemical Engineering, 34 (2017) 385-394.

[13] AOAC, Official Methods of Analysis, Association of Official Analytical Chemists, Washington, D. C., 2005.

[14] S. Paul, M.K. Das, P. Baishya, A. Ramteke, M. Farooq, B. Baroowa, R. Sunkar, N. Gogoi, Effect of high temperature on yield associated parameters and vascular bundle development in five potato cultivars, Scientia Horticulturae, 225 (2017) 134-140.

[15] P.J. Van Soest, J.B. Robertson, B.A. Lewis, Methods for Dietary Fiber, Neutral Detergent Fiber, and Nonstarch Polysaccharides in Relation to Animal Nutrition, Journal of Dairy Science, 74 (1991) 3583-3597.

[16] J.M. Castagnini, N. Betoret, E. Betoret, P. Fito, Vacuum impregnation and air drying temperature effect on individual anthocyanins and antiradical capacity of blueberry juice included into an apple matrix, LWT - Food Science and Technology, 64 (2015) 1289-1296.

[17] H.A. Barnes, A review of the slip (wall depletion) of polymer solutions, emulsions and particle suspensions in viscometers: its cause, character, and cure, Journal of Non-Newtonian Fluid Mechanics, 56 (1995) 221-251.

[18] J.F. Steffe, Rheological Methods in Food Process Engineering, 2 ed., Freeman Press, East Lansing, 1996.

[19] T.C. Polachini, L.F.L. Betiol, J.F. Lopes-Filho, J. Telis-Romero, Water adsorption isotherms and thermodynamic properties of cassava bagasse, Thermochimica Acta, 632 (2016) 79-85.

[20] E.C. Silva, M.P. Cereda, T.A.D. Colman, I.M. Demiate, E. Schnitzler, Characterisation of cassava bagasse in different granulometries from two starch processing plants, The Journal of Microbiology, Biotechnology and Food Sciences, 5 (2015) 99-102.

[21] C. Lu, J. Zhao, S.-T. Yang, D. Wei, Fed-batch fermentation for n-butanol production from cassava bagasse hydrolysate in a fibrous bed bioreactor with continuous gas stripping, Bioresource Technology, 104 (2012) 380-387.

[22] B. Volynets, F. Ein-Mozaffari, Y. Dahman, Biomass processing into ethanol: pretreatment, enzymatic hydrolysis, fermentation, rheology, and mixing, Green Processing and Synthesis, 6 (2017) 1-22.

[23] R. Glaser, Enzyme-based lignocellulose hydrolyzation—Sauter mean diameter of raw materials as a basis for cellulase performance characterization and yield prediction, Journal of Biotechnology, 214 (2015) 9-16.

[24] A.K. Chandel, F.A. Antunes, V. Anjos, M.J. Bell, L.N. Rodrigues, I. Polikarpov, E.R. de Azevedo, O.D. Bernardinelli, C.A. Rosa, F.C. Pagnocca, S.S. da Silva, Multi-scale structural and chemical analysis of sugarcane bagasse in the process of

sequential acid–base pretreatment and ethanol production by Scheffersomyces shehatae and Saccharomyces cerevisiae, Biotechnol Biofuels, 7 (2014) 63.

[25] A.P. Travalini, E. Prestes, L.A. Pinheiro, I.M. Demiate, Extraction and Characterization of Nanocrystalline Cellulose from Cassava Bagasse, Journal of Polymers and the Environment, (2017).

[26] F. Versino, O.V. López, M.A. García, Sustainable use of cassava (Manihot esculenta) roots as raw material for biocomposites development, Industrial Crops and Products, 65 (2015) 79-89.

[27] M. Odoch, E.M. Buys, J.R.N. Taylor, Mechanism of cassava tuber cell wall weakening by dilute sodium hydroxide steeping, Food Chemistry, 228 (2017) 338-347.

[28] S.A. EL-Sayed, M.E. Mostafa, Analysis of Grain Size Statistic and Particle Size Distribution of Biomass Powders, Waste and Biomass Valorization, 5 (2014) 1005-1018.

[29] P. Coussot, Rheometry of Pastes, Suspensions and Granular Materials – Application in Industry and Environment, John Wiley & Sons, Hoboken, New Jersey, 2005.

[30] D.J. Klingenberg, T.W. Root, S. Burlawar, C.T. Scott, K.J. Bourne, R. Gleisner, C. Houtman, V. Subramaniam, Rheometry of coarse biomass at high temperature and pressure, Biomass and Bioenergy, 99 (2017) 69-78.

[31] W. Hou, L. Zhang, J. Zhang, J. Bao, Rheology evolution and CFD modeling of lignocellulose biomass during extremely high solids content pretreatment, Biochemical Engineering Journal, 105 (2016) 412-419.

[32] N.-S. Roh, D.-H. Shin, D.-C. Kim, J.-D. Kim, Rheological behaviour of coal-water mixtures. 1. Effects of coal type, loading and particle size, Fuel, 74 (1995) 1220-1225.

[33] S. Viamajala, J.D. McMillan, D.J. Schell, R.T. Elander, Rheology of corn stover slurries at high solids concentrations – Effects of saccharification and particle size, Bioresource Technology, 100 (2009) 925-934.

[34] A.M. Gozzo, R.L. Cunha, F.C. Menegalli, Extensional and shear viscosity of acidified amaranth starch-sodium caseinate suspensions, Food Science and Technology (Campinas), 29 (2009) 587-596.

[35] C.M. Roche, C.J. Dibble, J.S. Knutsen, J.J. Stickel, M.W. Liberatore, Particle concentration and yield stress of biomass slurries during enzymatic hydrolysis at high-solids loadings, Biotechnology and Bioengineering, 104 (2009) 290-300.

[36] G. Laera, C. Giordano, A. Pollice, D. Saturno, G. Mininni, Membrane bioreactor sludge rheology at different solid retention times, Water Research, 41 (2007) 4197-4203.

[37] H. Chen, Q. Fu, Q. Liao, H. Zhang, Y. Huang, A. Xia, X. Zhu, Rheological properties of microalgae slurry for application in hydrothermal pretreatment systems, Bioresource Technology, 249 (2018) 599-604.

[38] C. Ségalen, E. Dieudé-Fauvel, J. Clément, J.C. Baudez, Relationship between electrical and rheological properties of sewage sludge – Impact of temperature, Water Research, 73 (2015) 1-8.

[39] N. Ouerfelli, Z. Barhoumi, O. Iulian, Viscosity Arrhenius Activation Energy and Derived Partial Molar Properties in 1,4-Dioxane + Water Binary Mixtures from 293.15 to 323.15 K, Journal of Solution Chemistry, 41 (2012) 458-474.

[40] M.K. Krokida, Z.B. Maroulis, G.D. Saravacos, Rheological Properties of Fluid Fruit and Vegetable Purree Products: Compilation of Literature Data, International Journal of Food Properties, 4 (2001) 179-200.

[41] V.D. Alves, F. Freitas, N. Costa, M. Carvalheira, R. Oliveira, M.P. Gonçalves, M.A.M. Reis, Effect of temperature on the dynamic and steady-shear rheology of a new microbial extracellular polysaccharide produced from glycerol byproduct, Carbohydrate Polymers, 79 (2010) 981-988.

[42] R.J. Farris, Prediction of the Viscosity of Multimodal Suspensions from Unimodal Viscosity Data, Transactions of The Society of Rheology (1957-1977), 12 (1968) 281-301.

Table 1. Chemical composition of the powdered cassava bagasse.

General composition	
Moisture (g·100 g^{-1} wet matter)	5.2 ± 0.1
Protein (g·100 g^{-1} dried matter)	1.37 ± 0.05
Fats (g·100 g^{-1} dried matter)	0.30 ± 0.05
Ash (g·100 g^{-1} dried matter)	1.12 ± 0.02
Total sugars (g·100 g^{-1} dried matter)	1.63 ± 0.03
Starch (g·100 g^{-1} dried matter)	49.5 ± 0.8
Fibers (g·100 g^{-1} dried matter)	46.1 ± 0.9
Fiber composition*	
Cellulose (g·100 g^{-1} dried fiber)	50.9 ± 0.5
Hemicellulose (g·100 g^{-1} dried fiber)	41.5 ± 0.4
Lignin (g·100 g^{-1} dried fiber)	7.69 ± 0.07

* Based on the values of NDF.

Table 2. Parameters of number-based and volume-based particle size distributions for powdered cassava bagasse.

Parameters	Average values	
	Number based	Volume based
$D_{0,1}$ (μm)	2.1	39.3
$D_{0,5}$ (μm)	2.9	155.5
$D_{0,9}$ (μm)	6.1	340.1
De Brouckere mean diameter – $D_{4,3}$ (μm)	119.7	175.5
Sauter mean diameter – $D_{3,2}$ (μm)	53.4	66.3
Span	1.401	1.935

Table 3. Fitting parameters of Herschel-Bulkley model for acid suspensions at intermediate conditions.

Temperature (K)	Parameters	Cassava bagasse concentration, X_S								
		2%			6%			10%		
		Acid concentration $[H_3PO_4]$, X_A								
		2%	6%	10%	2%	6%	10%	2%	6%	10%
278.13	τ_0 (Pa)	0.2944	0.7862	1.1915	0.9188	1.6739	2.5462	2.2481	2.7290	3.2157
	k (Pa·s^n)	0.3730	0.8157	1.2886	1.7530	2.0878	2.2757	4.1297	4.6276	4.9354
	n (-)	1.0033	1.0049	0.9999	0.9687	0.9559	0.9621	0.8889	0.8762	0.8509
	R^2_{adj}	0.9999	0.9999	0.9999	0.9999	0.9999	0.9998	0.9999	0.9999	0.9999
298.13	τ_0 (Pa)	0.2399	0.7788	1.1225	0.6610	0.7291	2.4177	1.1702	1.6657	2.1652
	k (Pa·s^n)	0.2965	0.7291	1.2204	1.0540	1.7695	1.6891	2.5929	3.0772	3.4120
	n (-)	0.9990	1.0058	0.9966	0.9809	0.9253	0.9686	0.8878	0.8767	0.8512
	R^2_{adj}	0.9999	0.9999	0.9999	0.9999	0.9994	0.9998	0.9999	0.9999	0.9999
318.13	τ_0 (Pa)	0.2376	0.6803	1.1625	0.4719	1.4434	1.7694	0.7119	1.2045	1.6431
	k (Pa·s^n)	0.2469	0.7073	1.1595	0.7370	1.0349	1.6120	1.7670	2.1613	2.6310
	n (-)	1.0019	0.9989	0.9988	0.9809	0.9864	0.9405	0.8938	0.8701	0.8531
	R^2_{adj}	0.9999	0.9999	0.9999	0.9999	0.9998	0.9987	0.9999	0.9999	0.9999

Table 4. Fitting parameters of an Arrhenius-type equation for apparent viscosity ($\eta_{app,10s^{-1}}$).

Cassava bagasse concentration, X_S (%)	Parameters	Acid concentration, X_A (%)					
		0	2	4	6	8	10
	A_0 (Pa·s)	9.82×10^{-7}	9.26×10^{-7}	1.03×10^{-6}	1.02×10^{-6}	2.52×10^{-6}	1.49×10^{-6}
0	E_a (kJ·mol^{-1})	17.22	17.36	17.24	17.26	15.10	16.40
	R^2_{adj}	0.9925	0.9919	0.9766	0.9793	0.9544	0.9953
	A_0 (Pa·s)	1.41×10^{-4}	4.34×10^{-4}	0.0240	0.0582	0.1326	0.0472
4	E_a (kJ·mol^{-1})	19.76	17.92	8.99	7.35	5.72	8.54
	R^2_{adj}	0.9995	0.8604	0.9858	0.9909	0.9651	0.9538
	A_0 (Pa·s)	6.08×10^{-4}	0.0023	0.0142	0.0256	0.0213	0.0916
6	E_a (kJ·mol^{-1})	18.16	15.31	11.23	10.14	10.86	7.49
	R^2_{adj}	0.9993	0.9953	0.9954	0.9907	0.9835	0.9758
	A_0 (Pa·s)	1.01×10^{-3}	0.0026	0.0066	0.0130	0.0223	0.0342
8	E_a (kJ·mol^{-1})	17.98	16.02	13.97	12.51	11.40	10.52
	R^2_{adj}	0.9995	0.9970	0.9982	0.9840	0.9958	0.9961
	A_0 (Pa·s)	1.50×10^{-3}	0.0029	0.0061	0.0075	0.0121	0.0236
10	E_a (kJ·mol^{-1})	17.84	16.38	14.66	14.35	13.27	11.74
	R^2_{adj}	0.9999	0.9964	0.9950	0.9916	0.9978	0.9951

Table S1. Fitting parameters of Herschel-Bulkley model for acid suspensions.

Temperature (K)	Parameters	Cassava bagasse concentration, X_S 0%						Cassava bagasse concentration, X_S 2%					
		Acid concentration [H_3PO_4], X_A						Acid concentration [H_3PO_4], X_A					
		0%	2%	4%	6%	8%	10%	0%	2%	4%	6%	8%	10%
278.13	τ_0 (Pa)	0.0000	0.0000	0.0000	0.0000	-0.0001	0.0000	0.0450	0.2944	0.5319	0.7863	0.9145	1.1915
	k (Pa·s^n)	0.0017	0.0017	0.0018	0.0018	0.0018	0.0018	0.1518	0.3730	0.6042	0.8157	1.0818	1.2886
	n (-)	0.9985	0.9995	0.9996	1.0003	0.9996	0.9997	1.0000	1.0033	1.0005	1.0049	0.9959	0.9999
	R^2_{adj}	1.0000	1.0000	1.0000	1.0000	1.0000	1.0000	1.0000	1.0000	1.0000	1.0000	1.0000	1.0000
288.13	τ_0 (Pa)	-0.0002	-0.0002	-0.0002	-0.0001	-0.0001	-0.0001	0.0458	0.2941	0.5737	0.6257	0.9571	1.6040
	k (Pa·s^n)	0.0013	0.0013	0.0014	0.0014	0.0014	0.0014	0.0977	0.3250	0.5280	0.8205	1.0194	1.1292
	n (-)	0.9968	0.9986	0.9990	0.9995	0.9988	0.9995	1.0108	1.0016	1.0124	0.9898	0.9997	1.0195
	R^2_{adj}	1.0000	1.0000	1.0000	1.0000	1.0000	1.0000	1.0000	0.9999	0.9999	0.9999	1.0000	0.9999
298.13	τ_0 (Pa)	-0.0001	-0.0001	-0.0002	-0.0001	0.0000	0.0001	0.0140	0.2399	0.4617	0.7788	0.9515	1.1225
	k (Pa·s^n)	0.0010	0.0010	0.0010	0.0010	0.0011	0.0011	0.0675	0.2966	0.5229	0.7291	0.9745	1.2204
	n (-)	0.9987	0.9976	0.9975	0.9984	1.0012	1.0015	1.0012	0.9990	1.0000	1.0058	1.0007	0.9966
	R^2_{adj}	1.0000	1.0000	1.0000	1.0000	1.0000	1.0000	1.0000	1.0000	1.0000	1.0000	1.0000	1.0000
308.13	τ_0 (Pa)	0.0000	0.0000	0.0001	0.0000	0.0001	0.0001	0.0044	0.2354	0.4659	0.6713	0.9549	1.2033
	k (Pa·s^n)	0.0008	0.0008	0.0009	0.0009	0.0008	0.0009	0.0418	0.2695	0.4954	0.7350	0.9396	1.1801
	n (-)	1.0009	1.0009	1.0011	1.0002	1.0008	1.0004	0.99895	0.99997	1.00023	0.99659	1.00257	0.99914
	R^2_{adj}	1.0000	1.0000	1.0000	1.0000	1.0000	1.0000	0.99999	0.99999	0.99999	0.99999	0.99999	0.99999
318.13	τ_0 (Pa)	0.0000	0.0000	0.0000	0.0000	0.0001	-0.0001	0.00398	0.23763	0.46276	0.68030	0.95586	1.16253
	k (Pa·s^n)	0.0007	0.0007	0.0008	0.0008	0.0008	0.0008	0.02181	0.24688	0.47494	0.70733	0.91370	1.15954
	n (-)	0.9990	0.9992	0.9991	0.9999	1.0024	0.9975	0.99999	1.00194	1.00023	0.99887	1.00342	0.99885
	R^2_{adj}	1.0000	1.0000	1.0000	1.0000	1.0000	1.0000	0.99999	0.99999	0.99999	0.99999	0.99999	0.99999

Table S1. Fitting parameters of Herschel-Bulkley model for acid suspensions (cont.).

Temperature (K)	Parameters	Cassava bagasse concentration, X_S 4%						Cassava bagasse concentration, X_S 6%					
		Acid concentration [H_3PO_4], X_A						Acid concentration [H_3PO_4], X_A					
		0%	2%	4%	6%	8%	10%	0%	2%	4%	6%	8%	10%
278.13	τ_0 (Pa)	0.2599	0.4495	0.9145	1.0956	1.8596	1.0317	0.6960	0.9188	2.8586	1.6739	0.7760	2.5462
	k (Pa·s^n)	0.6957	0.9602	1.0857	1.3575	1.3574	2.0760	1.5026	1.7530	1.4730	2.0878	2.8081	2.2757
	n (-)	1.0000	0.9879	0.9980	0.9805	1.0069	0.9334	0.9989	0.9687	1.0214	0.9559	0.9123	0.9621
	R^2_{adj}	0.9999	0.9999	0.9999	0.9999	0.9995	0.9987	0.9999	0.9999	0.9989	0.9999	0.9995	0.9998
288.13	τ_0 (Pa)	0.2314	0.5131	0.5280	0.8569	1.5400	1.4356	0.3276	0.8076	0.9696	1.1966	1.4638	1.4775
	k (Pa·s^n)	0.5158	0.7115	1.0247	1.2155	1.3048	1.6433	1.1906	1.3062	1.5926	1.7940	2.0352	2.3533
	n (-)	1.0015	1.0093	0.9868	0.9796	0.9894	0.9643	0.9886	0.9786	0.9561	0.9586	0.9506	0.9254
	R^2_{adj}	0.9999	0.9999	0.9999	0.9999	0.9999	0.9999	0.9999	0.9999	0.9999	0.9999	0.9999	0.9999
298.13	τ_0 (Pa)	0.1121	0.3466	0.8461	0.8630	0.6271	1.7135	0.4136	0.6611	0.9786	0.7291	2.1004	2.4177
	k (Pa·s^n)	0.4014	0.6272	0.7772	1.0703	1.5163	1.3401	0.8984	1.0540	1.2846	1.7695	1.5176	1.6891
	n (-)	0.9990	0.9970	1.0074	0.9813	0.9347	0.9958	0.9910	0.9809	0.9691	0.9252	0.9814	0.9686
	R^2_{adj}	0.9999	0.9999	0.9999	0.9999	0.9995	0.9999	0.9998	0.9999	0.9999	0.9994	0.9998	0.9998
308.13	τ_0 (Pa)	0.0803	0.3243	0.5423	0.7405	1.0065	1.9468	-0.0558	0.4676	0.8977	0.3457	1.6865	1.4404
	k (Pa·s^n)	0.3075	0.5300	0.7609	0.9914	1.2097	1.1813	0.8166	0.9371	1.1065	1.6454	1.3523	1.8294
	n (-)	1.0000	0.9999	0.9982	0.9779	0.9799	1.0078	0.9630	0.9654	0.9704	0.9096	0.9775	0.9332
	R^2_{adj}	0.9999	0.9999	0.9999	0.9999	0.9999	0.9993	0.9982	0.9999	0.9999	0.9993	0.9998	0.9999
318.13	τ_0 (Pa)	0.0621	0.0621	0.5196	0.7061	1.3139	1.3139	0.2200	0.4719	0.4472	1.4434	1.4753	1.7694
	k (Pa·s^n)	0.2349	0.2349	0.6900	0.9373	0.9975	0.9975	0.5640	0.7370	1.1339	1.0349	1.3775	1.6121
	n (-)	1.0019	1.0019	0.9899	0.9754	0.9958	0.9958	0.9910	0.9809	0.9333	0.9864	0.9446	0.9405

R^2_{adj}	0.9999	0.9999	0.9999	0.9999	0.9999	0.9999	0.9998	0.9999	0.9994	0.9998	0.9987	0.9987

Table S1. Fitting parameters of Herschel-Bulkley model for acid suspensions (cont.).

Temperature (K)	Parameters	Cassava bagasse concentration, X_S 8%						Cassava bagasse concentration, X_S 10%					
		Acid concentration [H_3PO_4], X_A						Acid concentration [H_3PO_4], X_A					
		0%	2%	4%	6%	8%	10%	0%	2%	4%	6%	8%	10%
278.13	τ_0 (Pa)	1.2434	1.5029	1.7428	1.9488	2.1958	2.3582	2.0172	2.2481	2.5864	2.7290	2.8890	3.2157
	k (Pa·s^n)	2.5922	2.8200	3.0452	3.2976	3.5105	3.7603	3.9539	4.1297	4.2587	4.6276	4.8015	4.9354
	n (-)	0.9467	0.9422	0.9331	0.9251	0.9172	0.9061	0.9019	0.8889	0.8779	0.8762	0.8598	0.8509
	R^2_{adj}	0.9999	0.9999	0.9999	0.9999	0.9999	0.9999	0.9999	0.9999	0.9999	0.9999	0.9999	0.9999
288.13	τ_0 (Pa)	0.8310	1.1086	1.3362	1.5162	1.7556	2.0732	1.3932	1.5755	1.8688	2.0819	2.3055	2.5388
	k (Pa·s^n)	1.9812	2.2287	2.4905	2.6319	2.9148	3.1205	3.0392	3.2856	3.3955	3.6324	3.8715	4.0748
	n (-)	0.9431	0.9441	0.9402	0.9141	0.9149	0.9099	0.9022	0.8918	0.8769	0.8667	0.8615	0.8503
	R^2_{adj}	0.9999	0.9999	0.9999	0.9999	0.9999	0.9999	0.9999	0.9999	0.9999	0.9999	0.9999	0.9999
298.13	τ_0 (Pa)	0.6121	0.8473	1.0247	1.2638	1.5065	1.8048	0.9804	1.1702	1.4505	1.6657	1.8925	2.1652
	k (Pa·s^n)	1.5454	1.7828	2.0379	2.2555	2.4805	2.6753	2.3847	2.5929	2.7382	3.0772	3.2096	3.4120
	n (-)	0.9481	0.9481	0.9328	0.9231	0.9159	0.9089	0.9022	0.8878	0.8749	0.8767	0.8595	0.8512
	R^2_{adj}	0.9999	0.9999	0.9999	0.9999	0.9999	0.9999	0.9999	0.9999	0.9999	0.9999	0.9999	0.9999
308.13	τ_0 (Pa)	0.4228	0.6548	0.8581	1.0956	1.3355	1.6314	0.6981	0.8985	1.1727	1.3866	1.6181	1.8855
	k (Pa·s^n)	1.2375	1.4307	1.7054	1.9325	2.1529	2.3617	1.8916	2.0678	2.3450	2.5340	2.7293	2.9747
	n (-)	0.9487	0.9322	0.9318	0.9241	0.9159	0.9099	0.9022	0.8818	0.8869	0.8697	0.8595	0.8562
	R^2_{adj}	0.9999	0.9999	0.9999	0.9999	0.9999	0.9999	0.9999	0.9999	0.9999	0.9999	0.9999	0.9999
318.13	τ_0 (Pa)	0.3121	0.5444	0.7821	0.9828	1.2206	1.5091	0.5098	0.7120	0.9925	1.2045	1.4493	1.6431

k (Pa·s^n)	0.9846	1.2212	1.4396	1.6845	1.9103	2.1081	1.5287	1.7670	1.9222	2.1614	2.3626	2.6310
n (-)	0.9471	0.9421	0.9343	0.9241	0.9169	0.9090	0.9032	0.8938	0.8782	0.8701	0.8603	0.8532
R^2_{adj}	0.9999	0.9999	0.9999	0.9999	0.9999	0.9999	0.9999	0.9999	0.9999	0.9999	0.9999	0.9999

Table S2. Analysis of variance (ANOVA) for yield stress:

Factor	Sum of squares	Degree of freedom	Mean square	F	p_{value}
T (linear)	6.92	1	6.92	85.84	<0.001
T (quadratic)	0.4714	1	0.4714	5.85	0.016
X_S (linear)	49.73	1	49.73	616.73	<0.001
X_S (quadratic)	0.3971	1	0.3971	4.92	0.027
X_A (linear)	23.97	1	23.97	297.27	<0.001
T (linear) × X_S (linear)	5.77	1	5.77	71.62	<0.001
X_S (linear) × X_A (linear)	1.70	1	1.70	21.12	<0.001
Error	13.87	172	0.08		
Total sum of square	102.83	179			

Table S3. Analysis of variance (ANOVA) for consistency coefficient:

Factor	Sum of squares	Degree of freedom	Mean square	F	p_{value}
T (linear)	19.12	1	19.12	545.84	<0.001
T (quadratic)	0.4887	1	0.4887	13.95	<0.001
X_S (linear)	183.99	1	183.99	5253.02	<0.001
X_S (quadratic)	2.68	1	2.68	76.44	<0.001
X_A (linear)	16.92	1	16.92	483.10	<0.001
T (linear) × X_S (linear)	14.69	1	14.69	419.36	<0.001
X_S (linear) × X_A (linear)	1.40	1	1.40	39.95	<0.001
Error	6.02	172	0.03		
Total sum of square	245.32	179			

Table S4. Analysis of variance (ANOVA) for flow index behavior:

Factor	Sum of squares	Degree of freedom	Mean square	F	p_{value}
X_S (linear)	0.3202	1	0.3202	2283.31	<0.001
X_S (quadratic)	0.0469	1	0.0469	334.25	<0.001
X_A (linear)	0.0139	1	0.0139	99.38	<0.001
X_S (linear) × X_A (linear)	0.0075	1	0.0075	53.36	<0.001
Error	0.0245	175	0.0001		
Total sum of square	0.4130	179			

Table S5. Analysis of variance (ANOVA) for apparent viscosity at shear rate of 10 s^{-1}:

Factor	Sum of squares	Degree of freedom	Mean square	*F*	p_{value}
T (linear)	15.20	1	15.20	508.16	<0.001
T (quadratic)	0.4205	1	0.4205	14.06	<0.001
X_S (linear)	120.47	1	120.47	4027.48	<0.001
X_A (linear)	13.70	1	13.70	458.27	<0.001
T (linear) × X_S (linear)	10.36	1	10.36	346.21	<0.001
X_S (linear) × X_A (linear)	0.2145	1	0.2145	7.17	0.008
Error	5.17	173	0.03		
Total sum of square	165.54	179			

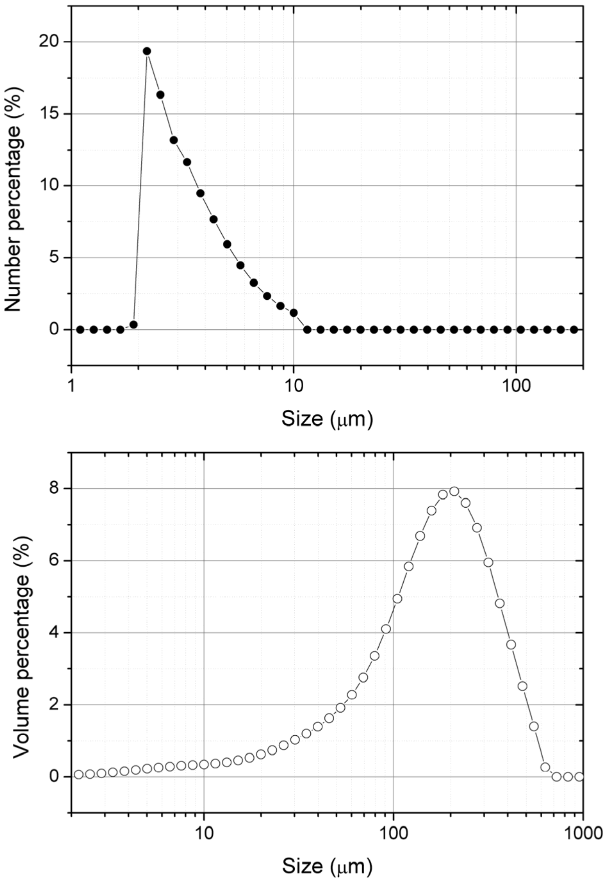

Figure 1. Number (A) and volume (B) based particle size distribution for powdered cassava bagasse.

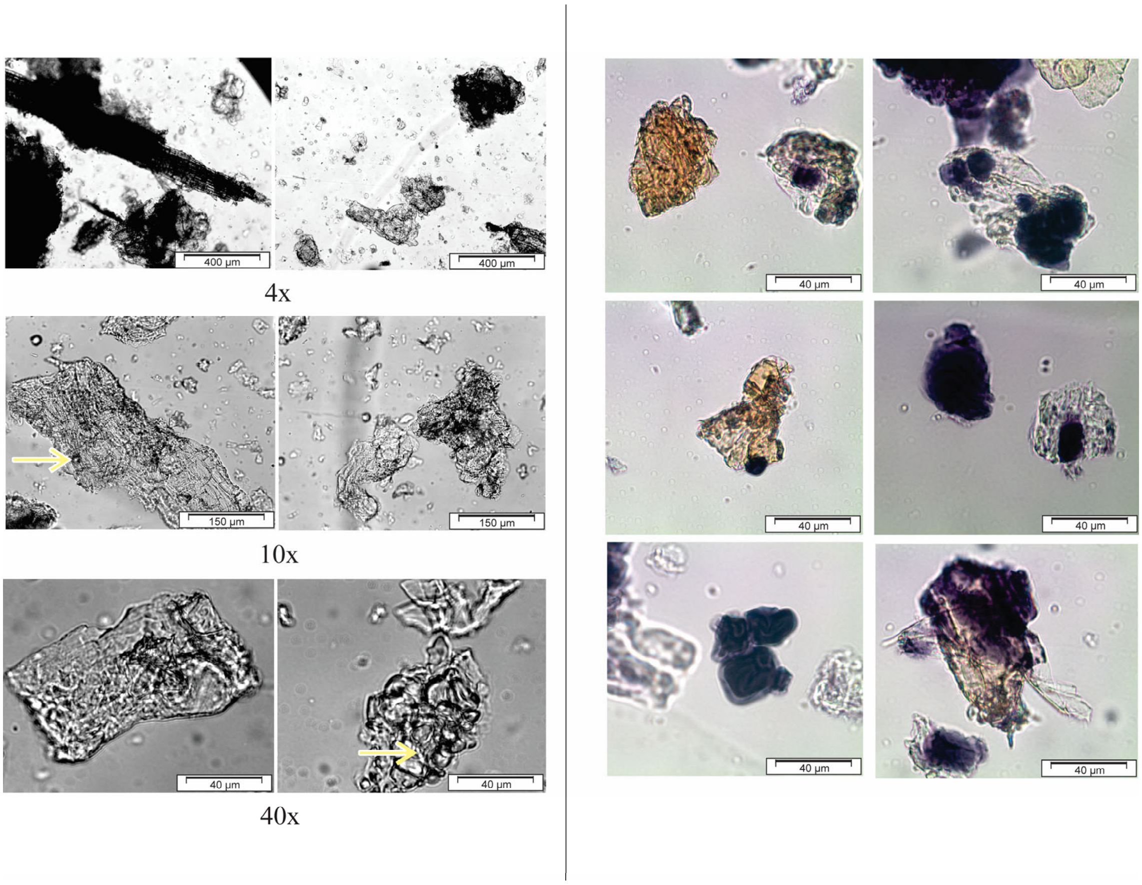

Figure 2. Optical microscopic images for cassava bagasse at 4x, 10x and 40x of magnification (A) and for cassava bagasse dyed with lugol at 40x of magnification (B).

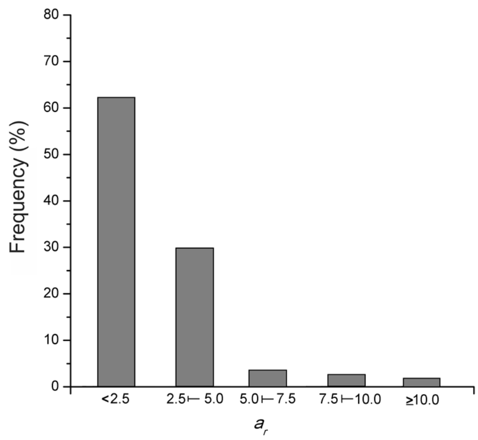

Figure 3. Distribution of the aspect ratio (a_r) values for powdered cassava bagasse particles.

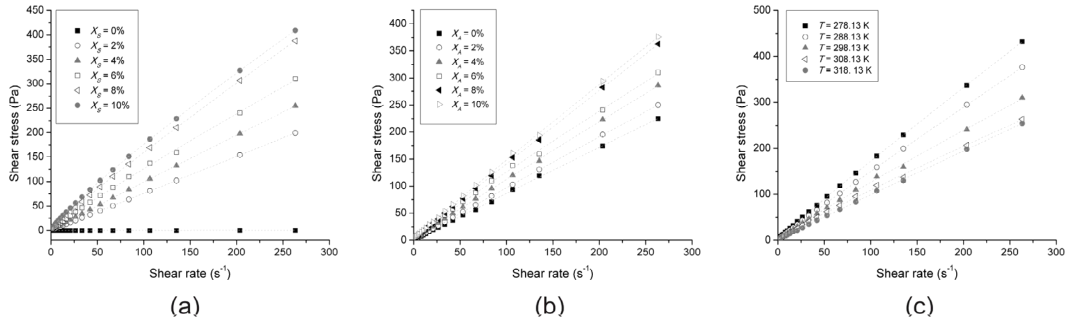

Figure 4. Rheograms of the acid suspensions containing cassava bagasse fitted to Herschel-Bulkley model. (a) X_A=6% at T=298.13 K; (b) X_S=6% at T=298.13 K; and (c) X_S=6% and X_A=6%.

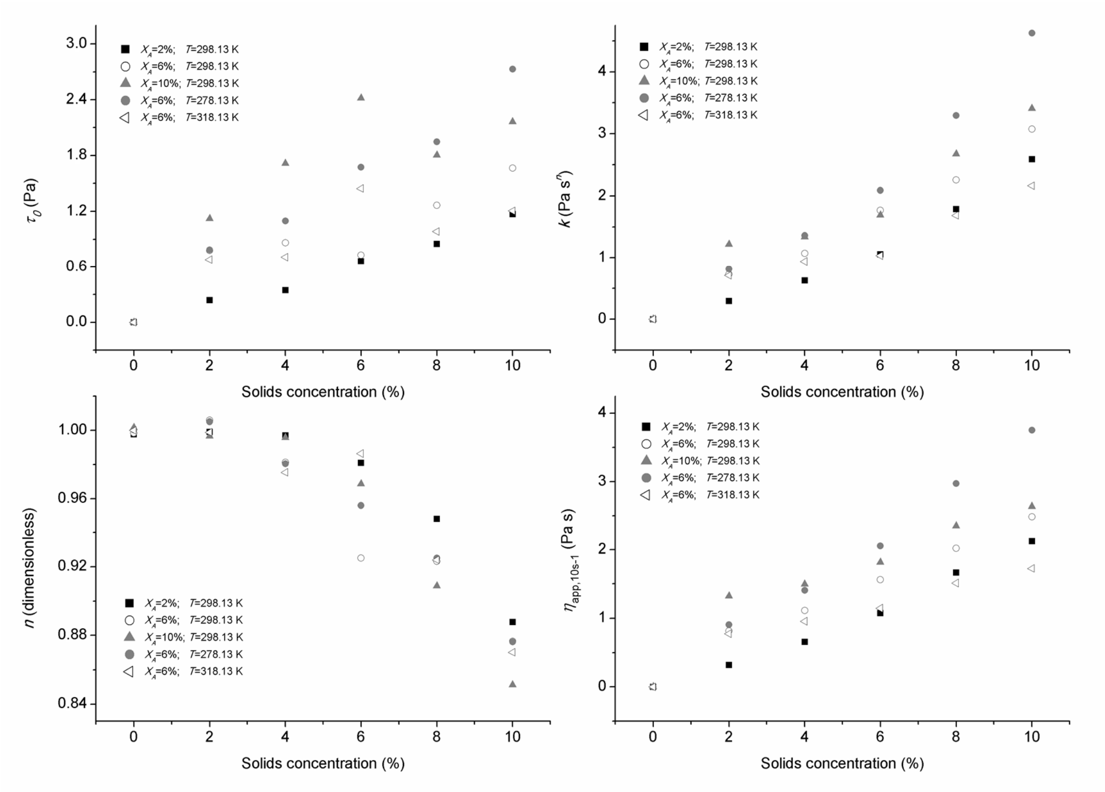

Figure 5. Yield stress (τ_0) (A), consistency coefficient (k) (B), flow behavior index (n) (C) and apparent viscosity ($\eta_{app,10s^{-1}}$) (D) as functions of cassava bagasse concentration at different acid concentrations and temperatures.

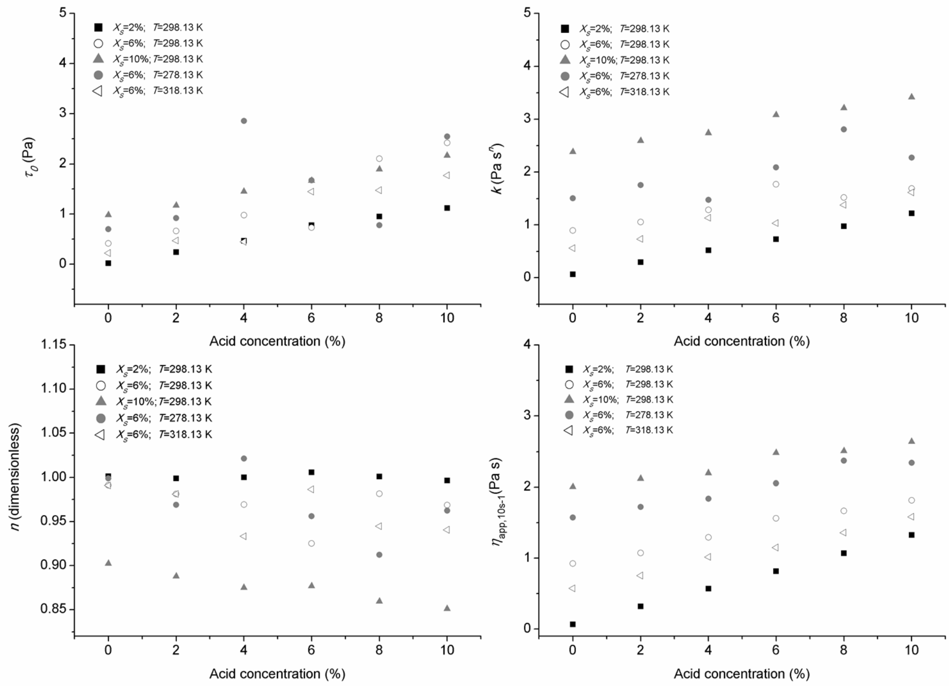

Figure 6. Yield stress (τ_0), consistency coefficient (k), flow behavior index (n) and apparent viscosity ($\eta_{app,10s^{-1}}$) as functions of phosphoric acid concentration at different solids concentrations and temperatures.

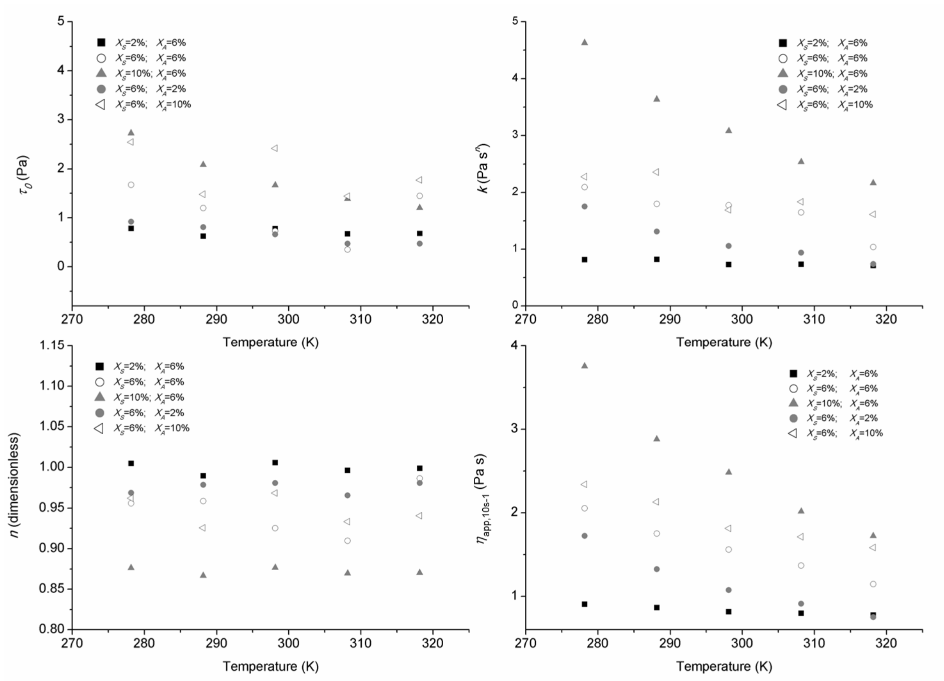

Figure 7. Yield stress (τ_0), consistency coefficient (k), flow behavior index (n) and apparent viscosity ($\eta_{app,10s^{-1}}$) as functions of absolute temperature at different acid and solids concentrations.